Alkali halide layers on W(110): Electron-stimulated desorption of ions, structure, and composition

U. Stawinski and E. Bauer
Physikalisches Institut, Technische Universität Clausthal, D-3392 Clausthal-Zellerfeld, Germany
(Received 6 July 1992; revised manuscript received 14 December 1992)

Electron-bombardment-induced alkali- and halogen-ion desorption from NaCl, KCl, KBr, KI, and CsI layers on W(110) are studied as a function of layer thickness from zero to several monolayers. The ion-energy distributions change with coverage which indicates the action of several desorption processes. The energy dependence of the ion yields shows that the primary step of these processes is the Knotek-Feibelman mechanism. Postemission neutralization is found to play an important role. The evolution of the ion yields with coverage contributes significantly to the understanding of the initial growth of the layers, which is obtained mainly from Auger electron spectroscopy and work-function-change measurements.

I. INTRODUCTION

Electron-stimulated desorption (ESD) of ions from surfaces is a challenging physical process with important applications and, therefore, has been the subject of numerous studies (for recent reviews see Refs. 1 and 2). In ESD from atomic and molecular adsorbates on metal and semiconductor surfaces the ionization process occurs in general in the adsorbed state which has been used with great success to obtain bonding geometry information from the ESD ion angular distribution.[2] For ionic crystal surfaces, however, calculations have shown that the probability of ion emission is significantly reduced if not suppressed by lattice relaxation around the ionized atom[3–5] which depends on the specific crystal structure and surface orientation. Thus for halides with rocksalt and fluorite structure no ESD of F^+ or Cl^+ ionized in or on the surface is expected.[1] Only after multiple ionization, which is improbable at low electron energies, is there a reasonable chance for the desorption of halogen ions. More likely is ionization of neutral species after desorption, a process which has been demonstrated experimentally.[6] In contrast to halogen ions X^+, an alkali ion M^+ can be desorbed if a halogen ion X^- below it is doubly ionized by an Auger process.[1,3–5] The kinetic energy of the M^+ ion is expected to be rather small, in agreement with the observation of Na^+ ions desorbed from a NaCl surface by electrons with energies above the ionization threshold of the Cl 3*s* level (18 eV).[7] In order to obtain Na^+ ESD below 30 eV it was necessary to damage the surface by preirradiation. Thus it appears that both M^+ and X^+ ESD are unlikely processes and that M and X ionization occur after desorption.

In the present work, which is part of a comprehensive study of alkali, halogen, and alkali halide layers on W(110) (Ref. 8) we eliminate the causes of the suppression of ESD ion emission and of ionization after desorption: lattice relaxation and efficient neutral desorption. Lattice relaxation occurs mainly within the first three atomic layers[1,3–5] and efficient neutral desorption[9] requires a bulk alkali halide crystal or at least a thick layer. By replacing the bulk alkali halide substrate below the first or first two layers by a metallic substrate the lattice relaxation, which is due to Coulomb and overlap (Pauli) repulsion in the ionic lattice, is significantly reduced and simultaneously the source of the neutral desorption (the bulk alkali halide) is eliminated. ESD ions should then be created primarily in the alkali halide layer. Indeed, we have observed some time ago very efficient ESD of Cl from KCl layers on W(110) but the charge state of the desorbed Cl was not analyzed at that time.[10] In the present study we measure the coverage and electron energy dependence of the M^+ and X^+ ESD yields as well as the M^+ and X^+ energy distributions not only for KCl but also for NaCl, KBr, KI, and CsI in order to obtain a better understanding of ion ESD from alkali halides.

II. EXPERIMENTAL SETUP AND PROCEDURE

The experimental setup has already been described.[11] The ultrahigh-vacuum system with a base pressure of 3×10^{-11} Torr allowed mass and energy analysis of the ESD ions with a quadrupole mass spectrometer and a cylindrical mirror analyzer (CMA), work-function-change ($\Delta\phi$) measurements and Auger electron spectroscopy (AES) using the internal gun of the CMA, low-energy electron diffraction (LEED), and secondary ion mass spectroscopy (SIMS).

The W crystal was oriented to within 0.05° of the (110) orientation, mounted on 1-mm-diam W rods, and could be quickly rotated into the various analysis and desorption positions. It was cleaned in the usual manner by heating at 1400 K in oxygen followed by flashing to 2200 K. Typical W:C and W:O Auger signal ratios after cleaning were 300:1. The alkali halide sources were quartz crucibles filled with pieces of alkali halide single crystals. Depositions were made in part cumulatively in small doses, in part continuously up to the desired coverage. Attempts to determine the coverage by AES combined with LEED failed because LEED showed only diffuse background, possibly due to disordering by the incident beam but possibly also because the layers had no long-

range order. Therefore the coverage was determined by comparison of the alkali halide AES signals with those of pure alkali and halogen layers. These were deposited from SAES getter sources and electrochemical cells, respectively, and were not influenced by the electron beam. All of them except Na layers have characteristic LEED patterns.[3] Thus combined AES and LEED measurements on these layers allowed us to calibrate the alkali and halogen coverages. Using these calibrations for the alkali halide layers implies that the different environment in these layers as compared to the pure alkali and halogen layers does not cause significant changes in the Auger peak shape and the angular distribution. Another uncertainty arises from the larger scatter of the AES data from the alkali halide layers due to the low current density and exposure which had to be used to minimize ESD during the AES measurements.

The ESD measurements with the CMA—ion-energy distributions and excitation functions—were made with a defocused 1–10 μA electron beam in normal incidence, with 300 eV energy for the energy distributions and 0–150 eV for the excitation functions. The ESD measurements with the mass spectrometer were made with a 300-eV, 1–5-μA electron beam incident at 45° onto the crystal which was biased +58 eV with respect to the mass spectrometer. For all ESD measurements individual doses were used. The absence of ESD from pure alkali and halogen layers was verified by prolonged bombardment with a 10-μA, 300-eV electron beam focused to a diameter of about 25 μm and subsequent AES. The Auger signal decrease after one hour bombardment was less than 1–10 % in the various layers, which corresponds to desorption cross sections of less than 10^{-34}–10^{-33} cm^2.

The AES measurements were made with a 2-μA, 2-keV electron beam, using individual doses for each coverage. In order to minimize the influence of ESD all Auger peaks were recorded five times and their amplitudes extrapolated to zero bombardment time. The alkali and halogen layers could be measured cumulatively with a 5-μA beam due to the absence of ESD. The following Auger peaks were used for the various atoms: Na $KL_{23}L_{23}$ (990 eV), K $L_3M_{23}M_{23}$ (252 eV), Cs $M_5N_{45}N_5/M_4N_{45}N_5$ (563 eV/575 eV), Cl $L_3M_{23}M_{23}$ (181 eV), Br $M_3M_{45}N_{23}$ (102 eV) and I $M_5N_{45}N_{45}$ (511 eV). The W $N_{45}N_{67}N_{67}$ (163–179 eV) group was used as a reference in order to allow quantitative comparisons of the results obtained over an extended period. In the $\Delta\phi$ measurements with the coaxial CMA gun the electron beam energy was 15 eV, the saturation current of the clean surface was 300 nA, and the sample was biased to a constant current of 30 nA. The bias difference between clean and adsorbate covered surface gives $\Delta\phi$ with an accuracy of $\pm$5 meV.

III. RESULTS

Only part of the results can be presented here, mainly the coverage dependence of the AES and $\Delta\phi$ data, which are essential for the understanding of the coverage dependence of the ESD results, the main topic of this study. The primary electron energy dependence of the ion yields, the ion-energy distribution, and the dependence of the ion yields on bombardment time and layer composition will be illustrated only by examples. For each layer material we first present the AES and $\Delta\phi$ data from which we derive models of the growth and structure of the layers. The results are plotted as a function of the number of deposition doses in arbitrary units which are identical in all figures for a given material. The AES signals are also plotted in arbitrary units which are identical for a given alkali or halogen, irrespective of its partner in the compound. These units can be compared directly with the coverages deduced from combined AES and LEED studies of the pure alkali or halogen layers. The symbols nM, nX (n=0,4,5; M=Na,K,Cs; X=Cl,Br,I) on the left side of the AES signal plots give the number density of the adsorbed M and X atoms in $n\times10^{14}$ atoms/cm^2 as obtained from the calibration with the pure layers, assuming no attenuation by a second layer. The Cl, Br, I, and Na AES signals do not go to zero at zero dose because no background subtraction was made.

A. NaCl

Figure 1 shows the AES and $\Delta\phi$ data for NaCl, the most difficult of the materials studied because of the low sensitivity of AES for Na. Combined with strong ESD, this causes the large error bars seen in the figure. The deviation of the Na data from a straight line below about 100 doses is, however, reproducible. We start our analysis at 200 doses where all curves show a change of slope. Using the calibration on the left side and assuming no attenuation we obtain 8.75×10^{14} Cl atoms/cm^2 while the Na error bars allow values ranging from 6.8×10^{14} to 7.9×10^{14} Na atoms/cm^2. Such large atomic densities, $(15.55-16.65)\times10^{14}$ atoms/cm^2, are not possible in a NaCl monolayer (ML). Therefore we attribute the slope changes to the completion of a double layer. This re-

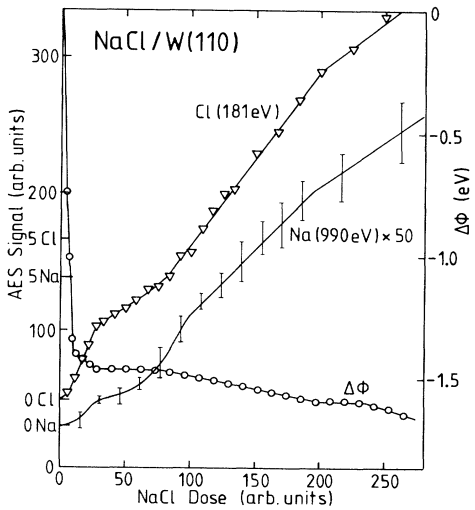

FIG. 1. Work-function change, Cl 181-eV and Na 990-eV Auger electron signals as a function of NaCl exposure of W(110). In this and the subsequent figures many data points were omitted in regions of small point spacing for the sake of clarity.

quires correction for attenuation. 180-eV electrons are typically attenuated by a factor κ of about 0.6 by a monolayer on top of the emitter (inelastic mean free path $\lambda=6.6$ Å, layer thickness 2.5 Å). Thus the total Cl coverage at 200 doses is $N_{\mathrm{Cl}}^{2}\approx 8.75\times10^{14}\times2/(1+\kappa)=10.95\times10^{14}$ atoms/cm^2. For Na the attenuation $\beta=(1+\kappa)/2$ could be obtained directly from the pure Na layers which grow at least initially ML by ML. With the β value 0.94 derived in this manner one obtains $N_{\mathrm{Na}}^{2}\approx(7.0-8.2)\times10^{14}$ atoms/cm^2. This gives a $N_{\mathrm{Na}}^{2}:N_{\mathrm{Cl}}^{2}$ ratio of $0.64-0.75\approx2:3-3:4$ for the double layer, clearly not 1:1 as expected from the composition of the vapor.

In order to understand this unexpected result we consider first in more detail the Cl data. The slope changes in Fig. 1 can be due to changes in sticking coefficient α, in AES angular distribution, in AES peak shape, or in AES signal attenuation β caused by structural changes. We assume here that only the first and last causes occur. If N is the flux of the NaCl molecules (in arbitrary units) then the apparent numbers of Cl atoms adsorbed in the three segments 0–28, 28–80, 80–200 doses in Fig. 1 are $N_1^{\mathrm{Cl}}=28\alpha_1^{\mathrm{Cl}}N=3.1\times10^{14}$, $N_2^{\mathrm{Cl}}=52\alpha_2^{\mathrm{Cl}}\beta_2^{\mathrm{Cl}}N=1.0\times10^{14}$, and $N_3^{\mathrm{Cl}}=120\alpha_3^{\mathrm{Cl}}\beta_3^{\mathrm{Cl}}N=4.65\times10^{14}$ atoms /cm^2. Assuming $\alpha_1^{\mathrm{Cl}}=1$ gives $N=0.111\times10^{14}$. With this value we obtain $\alpha_2^{\mathrm{Cl}}\beta_2^{\mathrm{Cl}}=0.174$ and $\alpha_3^{\mathrm{Cl}}\beta_3^{\mathrm{Cl}}=0.35\approx2\alpha_2^{\mathrm{Cl}}\beta_2^{\mathrm{Cl}}$. With $\beta_3^{\mathrm{Cl}}=(1+\kappa^{\mathrm{Cl}})/2=0.8$ one obtains $\alpha_3^{\mathrm{Cl}}\approx0.44$. β_2^{Cl} follows from the condition that the sum of the attenuation-corrected N_i^{Cl} values, $\sum_{i=1}^{3}\mathring{N}_i^{\mathrm{Cl}}=\sum_{i=1}^{3}N_i^{\mathrm{Cl}}/\beta_i$, must be equal to N_{Cl}^{2}. This gives $\beta_2^{\mathrm{Cl}}\approx0.49$ and from this $\alpha_2^{\mathrm{Cl}}\approx0.36$. Similarly, one obtains for the segments 0–28 and 100–200 doses $N_1^{\mathrm{Na}}=28\alpha_1^{\mathrm{Na}}N=1.55\times10^{14}$ and $N_3^{\mathrm{Na}}=100\alpha_3^{\mathrm{Na}}\beta_3^{\mathrm{Na}}N=(3-4.2)\times10^{14}$ atoms/cm^2. A comparison of N_1^{Cl} and N_1^{Na} shows that at least up to about 30 doses the ratio of adsorbed Na:Cl is only 1:2, while between 100 and 200 doses the apparent numbers (uncorrected for attenuation) are the same within the large limits of error: $N_3^{\mathrm{Na}}\approx(100/120)N_3^{\mathrm{Cl}}$. This means $\alpha_3^{\mathrm{Na}}\beta_3^{\mathrm{Na}}\approx\alpha_3^{\mathrm{Cl}}\beta_3^{\mathrm{Cl}}=0.35$ or $\alpha_3^{\mathrm{Na}}\approx0.37$ with $\beta_3^{\mathrm{Na}}=0.94$. In the transition region (28–100 doses) it is difficult to separate sticking and restructuring effects and no attempt will be made to do so.

Important additional information is provided by the $\Delta\phi$ results whose most striking aspect is the rapid decrease at very low coverages and its sudden transition at ten doses to a much smaller change. Assuming constant sticking up to 28 doses this transition occurs at a coverage of 0.55×10^{14} Na and 1.1×10^{14} (Cl atoms)/cm^2. If all atoms were separate and had the same dipole moment as in the pure Na and Cl layers at the same coverages, a $\Delta\phi$ of -1.10 eV would be expected. The observed change $\Delta\phi=-1.4$ eV is much larger, which can only be explained if the Na and Cl atoms form dipoles which are not parallel to the surface. There are two possibilities: (i) the layer consists of 0.55×10^{14} (NaCl molecules)/cm^2 and an equal number of Cl atoms or (ii) the layer consists of 0.55×10^{14} ($NaCl_2$ molecules)/cm^2. This molecule of course does not exist in the gas phase but the ionic molecule $NaCl_2^-$ is found in the secondary ion (SI) spectrum of NaCl layers.[8] In order to have a significant positive dipole moment in the adsorbed state, this molecule cannot be linear but must be bent with the Cl pointing towards the substrate. The normal component $p_\perp$ of the dipole moment of the $NaCl_2$ molecules must account for a $\Delta\phi=-1.40$ eV, that of the NaCl molecules only for $\Delta\phi=-1.32$ eV because the remaining Cl atoms contribute $\Delta\phi=-0.08$ eV. From the relation $\Delta\phi=-4\pi en$ we obtain $p_\perp^{\mathrm{NaCl_2}}=6.75$ debye (D) and $p_\perp^{\mathrm{NaCl}}=6.4$ D which can be compared with the dipole moment of the free molecule, $p^{\mathrm{NaCl_2}}=13.9$ D.[12] The much smaller value of $p_\perp^{\mathrm{NaCl}}$ can have several causes: reduction of the charge on the Cl by bonding to the substrate, tilt, and/or hindered rotation of the molecule. The sudden slower linear $\Delta\phi$ decrease from ten to 28 doses requires a sudden transition to a much smaller dipole moment. We attribute this linear region to the formation and growth of monolayer $NaCl_2$ islands. The subsequent linear regions coincide well with the corresponding segments of the Cl AES curves.

The combination of all these results leads to the following model of the growth and structure of the layer. Upon adsorption partial loss of Na occurs, initially of 50% Na. The Cl atoms left behind form together with the surviving NaCl molecules a two-dimensional (2D) gas with the NaCl or $NaCl_2$ dipoles normal or, at least, nonparallel to the surface, with Na pointing outward. At a critical coverage (ten NaCl doses) these dipoles flip over parallel to the surface and form with the Cl atoms 2D $NaCl_2$ islands. These islands become unstable at another critical coverage (30 doses) and rearrange into double layer islands. This process extends up to 80 doses, and causes little $\Delta\phi$ change and a much smaller growth rate of the AES signals, which is partially also due to a decrease of the Cl sticking coefficient. The completion of this rearrangement is followed by lateral growth until completion of the double layer, with comparable—within the limits of error of the Na coverage determination possibly identical—sticking coefficients for Na and Cl. The coverage dependence of the sticking coefficients causes a transition from the composition $NaCl_2$ in the ML islands to the composition Na_2Cl_3 or Na_3Cl_4 at 2 ML (200 doses). Whether NaCl deposited in excess of 2 ML grows ML by ML on this transition layer or as flat 3D crystals cannot be decided with certainty because of the limited number of AES data beyond 2 ML.

With this information at hand the coverage dependence of the ESD signals can be presented and analyzed. Figure 2 shows the Na^+ and Cl^+ ESD signals as observed with the mass spectrometer (23 and 35 amu). The energies are the peak energies in the energy distributions measured with the CMA. CMA and mass spectrometer signals were correlated via their dependence upon NaCl exposure and bombardment time. Up to ten doses, i.e., in the 2D molecular phase, no Cl^+ is observed but a strong, sharply peaked Na^+ signal which disappears again shortly above ten doses. The exposure dependence of this initial alkali-ion ESD signal will be analyzed later in conjunction with the K^+ signal from KI layers. With the onset of condensation at ten doses a new Na^+ signal develops which rises linearly up to 33 doses. The superposition of the decreasing Na^+ signal from the 2D gas phase and of the increasing Na^+ signal from the 2D condensate

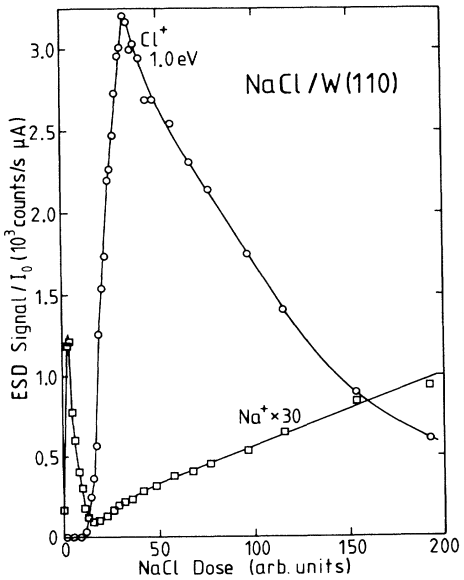

FIG. 2. ESD signals from NaCl layers on W(110) as a function of NaCl exposure. Exposure range: 2 ML. The energies in this and later figures are the energies at which the maxima in the energy distributions shown in Fig. 4 occur.

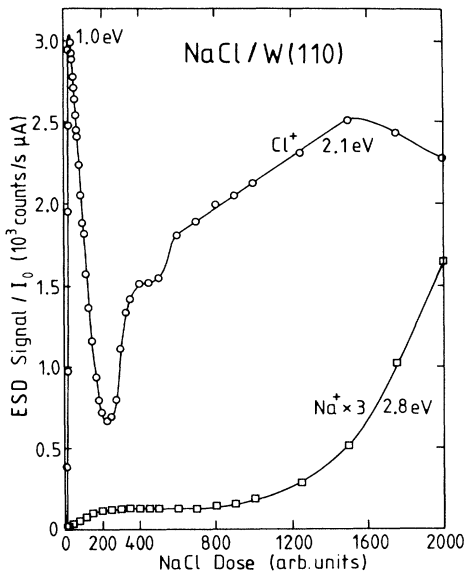

FIG. 3. ESD signals from NaCl layers on W(110) as a function of NaCl exposure up to 20 ML.

phase which has been measured with much more points than shown in Fig. 2 causes the minimum seen in the figure. Upon condensation a very strong Cl^+ ESD signal appears which grows rapidly to a sharp maximum at 33 doses. From ten to about 15 doses, the exposure range in which the Na^+ signal from the 2D gas disappears, the Cl^+ signal rises less rapidly. This transition region is attributed to the nucleation stage of the 2D $NaCl_2$ condensate. Above 33 doses the Cl^+ signal decreases rapidly and the Na^+ signal increases more slowly. This is connected with the transition from monolayer to double layer islands and their lateral growth. The difference between the transition exposures deduced from AES and ESD, 28 versus 33, is mainly due to slow changes of the dose size over extended measurement periods.

For NaCl an attempt was made to approach the behavior of bulk NaCl. For this purpose the NaCl exposure was increased up to 2000 doses, which corresponds to about 20 ML for constant sticking coefficient. The ESD results are shown in Fig. 3. The Na^+ signal saturates around 300 doses (3 ML), remains nearly constant up to 700 doses (7 ML), and subsequently increases exponentially in the exposure range measured. The exposure dependence of the Cl^+ signal is more complicated. The 1.0-eV signal disappears above 200 doses (2 ML) and is replaced by a 2.1-eV Cl^+ signal. The superposition of the two signals produces the deep minimum at about 2 ML. The new signal saturates at about 4 ML, rises again rapidly at about 5 ML, grows linearly from 6 to about 15 ML, and then decreases. The energy difference between the low- and high-coverage Cl^+ ESD signals indicates different environments of the excited Cl species before emission. It appears likely that above 2 ML the layer has stoichiometric NaCl composition. Whether the growth of 3D NaCl crystal starts at 2 ML or above 4 ML cannot be decided on the basis of the available data. In any case, ESD of ions with hyperthermal energies is observed even at 20-ML average thickness, that is significantly above the transition layer which is 2 ML—or possibly 4 ML—thick.

The energy distributions of these ions are shown in Fig. 4 for the 1.0-eV peak at 30 doses, i.e., close to its maximum yield and for the 2.1-eV peak at 600 doses. They were recorded sequentially without interruption from 0 to 4 eV and 0 to 7 eV, respectively, and show the decrease and conversion of the ESD-active species. In Fig. 4(b) the 2.8-eV Na^+ signal—identified as Na^+ with the mass spectrometer via its bombardment time dependence—is

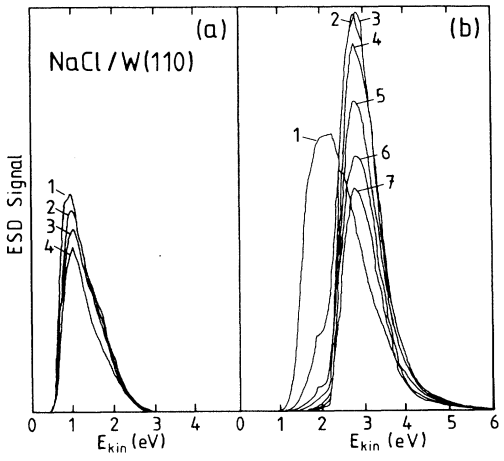

FIG. 4. ESD ion energy distributions from NaCl layers on W(110). (a) 30 doses (1.0-eV Cl^+ maximum in Fig. 2), (b) 600 doses (2.1-eV Cl^+ and 2.8-eV Na^+ ions in Fig. 3). The numbers show the sequence in which the spectra were recorded during continuous electron bombardment.

initially buried in the high-energy side of the 2.1-eV Cl^+ peak which decreases rapidly with bombardment time while the Na^+ grows rapidly (1→2) and then decreases slowly (2→7). It should be remembered that the ESD ion signals shown in Figs. 2 and 3 are the values extrapolated to zero bombardment time. Figure 4 illustrates the importance of this extrapolation for the study of the virgin state of the layers.

The dependence of the ESD ion yields on the energy of the electron beam is shown in Fig. 5 for the 1.0-eV Cl^+ signal. Within the limits of error the threshold is at the ionization energy of the Cl 3*s* level. An additional yield increase is indicated at the Na 2*p* ionization energy. The threshold for the 2.1-eV Cl^+ and the 2.8-eV Na^+ signals (not shown) is also at the Cl 3*s* ionization energy but no additional increase is seen at the Na 2*p* level and the signals continue to rise above 50 eV. These results clearly show that ESD ion emission is a consequence of inner shell ionization, the prerequisite of an Auger process, which produces the electronic excitation energy necessary for ion emission. Apparently Cl^+ emission from the initial condensate ($NaCl_2$ ML islands) is not only caused by an intra-atomic Auger process but also by an interatomic Auger transition (Na 2*p* threshold) which is ineffective in thicker layers. Na^+ emission is caused by an interatomic Auger transition (Cl 3*s* threshold, no effect of Na 2*p* threshold), at least in the energy range studied ($E \lesssim 70$ eV). No excitation function was measured for the Na^+ signal from the 2D gas but it appears likely that it is also caused by an interatomic Auger transition involving the 3*s* hole in a Cl atom below the Na atom. An alternative explanation of the increase of the ESD ion yields above inner shell excitation thresholds is an increase in the emission of secondary electrons which could increase ionization of ESD neutrals. Arguments which speak against this mechanism will be given in the discussion.

B. KCl

The AES data of KCl (Fig. 6) are apparently quite different from those of NaCl (Fig. 1): the AES signal has

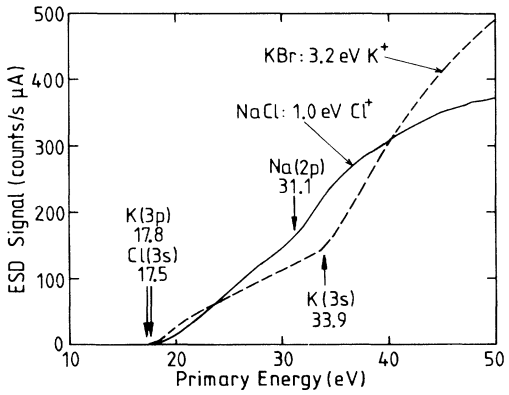

FIG. 5. ESD excitation functions of 1.0-eV Cl^+ ions from NaCl and of 3.2-eV K^+ ions from KBr layers on W(110). The vertical arrows indicate the various core-level ionization energies.

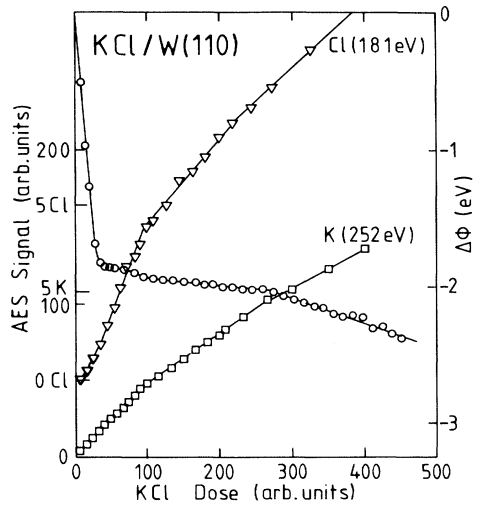

FIG. 6. Work-function change, Cl 181-eV and K 252-eV Auger electron signals as a function of KCl exposure.

three linear segments with monotonically decreasing slope. The $\Delta\phi$ data, however, are quite similar. The first slope changes of the AES signals at 100 KCl doses occur at coverages of 2.25×10^{14} (K atoms)/cm^2 and 4.6×10^{14} (Cl atoms)/cm^2, which gives a K:Cl ratio of $\approx$1:2 for this layer, that is the same composition as that of the NaCl ML islands. The transition to the double layer, however, takes place at a much larger coverage, 6.85×10^{14} atoms/cm^2, compared to 4.65×10^{14} atoms/cm^2 in NaCl layers and involves no initial reorganization of the first layer. This follows from the constant AES slope all the way up to the completion of the double layer at about 250 doses. If the sticking coefficients for K and Cl were constant from 0 to 250 doses one would expect 5.6×10^{14} (K atoms)/cm^2 and 11.5×10^{14} (Cl atoms)/cm^2 at 250 doses. With κ values of 0.6 for Cl (181 eV) and 0.7 for K (252 eV) Auger electrons one obtains from the AES signals at 250 doses 5.4×10^{14} (K atoms)/cm^2 and 8.8×10^{14} (Cl atoms)/cm^2. The value for K agrees within the limits of error with the expected value but for Cl the sticking probability in the second layer is apparently only about $(8.8-4.6)/(11.5-4.6)\approx0.6$ of that in the first layer. This lead to an average composition K_3Cl_5 of the double layer. If no additional K is incorporated into the first (KCl_2) layer then the second layer has the composition K_3Cl_4. Thus, similar to NaCl, KCl also forms on W(110) an alkali-deficient transition double layer. The slope of the third AES signal segment is so large that formation of 3D KCl crystals can be excluded. Whether or not the third layer is also still K deficient cannot be deduced from the available data.

From the $\Delta\phi$ data again a very large dipole moment of the species adsorbed up to about 30 doses may be deduced. For constant sticking coefficients up to 100 doses 0.68×10^{14} (K atoms)/cm^2 and 1.38×10^{14} (Cl atoms)/cm^2 are adsorbed at 30 doses. Assuming that they have the same dipole moments as in the pure K and Cl layers at this coverage the expected $\Delta\phi$ is $-(1.5+0.2)$ eV which is less than the observed value of 1.8 eV. This

leads to the same conclusion as in the case of NaCl: initially a molecular gas phase with a strong normal component of the dipole moment, here $p_{\perp}^{KCl}=6.5$ D ($p=18.4$ D for the free KCl molecule) or $p_{\perp}^{KCl_2}=6.9$ D, forms which is stable up to a somewhat larger coverage than in NaCl layers, $\approx 0.7\times10^{14}$ (KCl_2 molecules)/cm (30 doses) versus 0.55×10^{14} ($NaCl_2$ molecules)/cm^2, or the corresponding NaCl (KCl) and Cl coverages. Above this coverage the dipoles flip over to become parallel to the surface, forming 2D KCl_2 islands until the first monolayer with the composition KCl_2 and total atomic density 6.85×10^{14}/cm^2 is completed. This is followed by the formation of a second layer with a total double layer coverage of 14.2×10^{14} atoms/cm^2 and average composition K_3Cl_5, possibly with KCl_2 in the first and K_3Cl_4 in the second layer. The third layer grows also by the ML-by-ML mode.

The exposure dependence of the KCl ESD ion yields (Fig. 7) can be analyzed now. The alkali-ion peak at very small exposures is missing, probably not because it does not exist but rather because insufficient data were taken in this exposure range of KCl layers which were the first to be studied. The K^+ secondary ion yield shows a clear local maximum in this exposure range[8] in accordance with NaCl, KBr, and KI which all produce a strong Na^+ or K^+ ESD signal at low exposures. The Cl^+ signal appears at about 30 doses, that is with the onset of 2D KCl_2 layer formation, and rises linearly until completion of this layer at 100 doses. With the start of the second layer a second Cl^+ peak forms which can be distinguished from the first peak by its different energy distribution maximum (2.2 eV versus 1.5 eV). The superposition of the two peaks in the mass spectrometer, which is schematically indicated in Fig. 7, leads to an only poorly pronounced minimum. The K^+ ESD signal appears at the beginning of the second monolayer. Similar to Na^+ from NaCl layers, the K^+ ions have a large energy, with the peak of the energy distribution at 3.0 eV.

The thresholds for the 2.2-eV Cl^+ and the 3.0-eV K^+ ESD are at about 18 eV. The Cl 3*s* and K 3*p* ionization energies are 17.5 and 17.8 eV, respectively, so that no decision can be made which of the primary holes (Cl 3*s* or K 3*p*) is responsible for the Auger process leading to ion emission. Although the 3.0-eV K^+ signal increases more rapidly above the K 3*s* ionization energy (33.9 eV), no clear threshold behavior is seen at this energy. In analogy with NaCl, it appears reasonable to assume the primary hole for both 2.2-eV Cl^+ and 3.0-eV K^+ emission in the Cl 3*s* level and no significant contribution from holes in the K 3*s* level.

The influence of the bombardment time on the ESD yields is shown in Fig. 8 for two exposures, 90 doses [≈ 1 ML (a)] and 400 doses (b). The K and Cl AES signal changes accompanying the ESD yield change are also plotted for the 90-dose exposure. The bombardment time has been scaled appropriately to account for the difference in energy and current density between AES and ESD measurements. The K(251 eV) AES signal is unaffected by the bombardment while the Cl(181 eV) AES signal decreases nearly exponentially to 66 arbitrary units, the value at which Cl^+ ESD sets in (at 30 doses) with increasing deposition time. Thus Cl is not desorbed completely. The final composition of the layer is stoichiometric KCl and the total atomic density 4.0×10^{14} atoms/cm^2. Interestingly, the Cl^+ ESD signal decreases initially only slowly in spite of the rapid de-

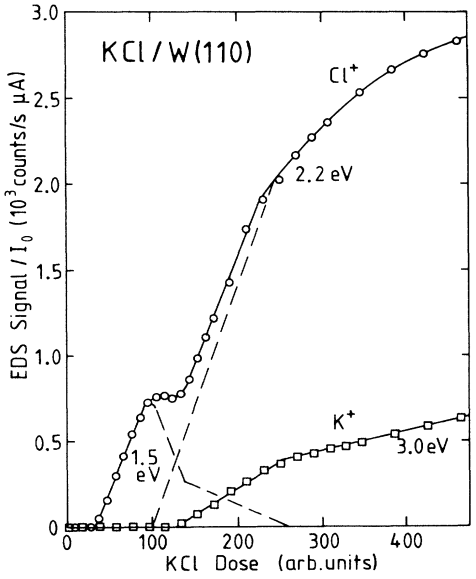

FIG. 7. ESD signals from KCl layers on W(110) as a function of KCl exposure. The dashed lines indicate the probable separation of the Cl^+ signal into the two Cl^+ states which, however, was not studied in detail.

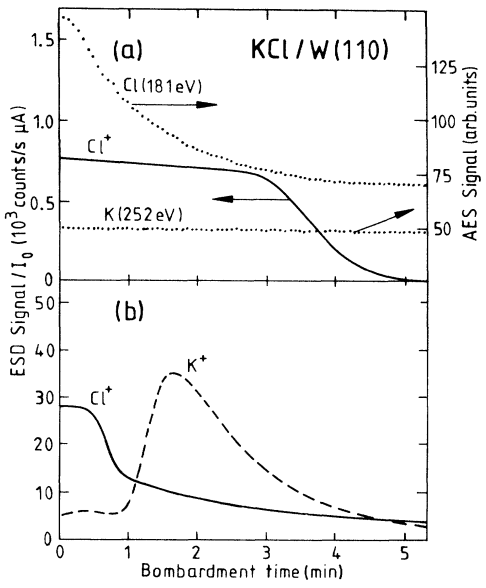

FIG. 8. Dependence of the ESD signals upon bombardment time for (a) a monolayer and (b) a thick layer. In (a) also the bombardment time dependence of the Cl and K Auger electron signals is shown which was scaled in time to account for the different ESD rates due to differences in energy and current between ESD and AES measurements.

crease of the Cl coverage while its final rapid decrease to zero is accompanied by an only small coverage change. Normalized to the still present Cl coverage the Cl^+ ESD yield increases with decreasing Cl coverage to a maximum at 2.25×10^{14} (Cl atoms)/cm^2 ($\approx K_9Cl_{10}$) and drops then precipitously to zero at 2.0×10^{14} (Cl atoms)/cm^2 (NaCl). Obviously small deviations from stoichiometry can cause strong ESD of ions. The influence of bombardment time on ion ESD at 400 NaCl doses shows the typical behavior observed in all alkali halides at higher coverages: initially Cl^+ ESD dominates but decreases rapidly to a lower ESD yield range. The decrease of the Cl^+ signal is followed by a rapid increase of the K^+ signal which dominates temporarily the Cl^+ signal but decreases subsequently more rapidly. Figure 8(b) is a good illustration of the importance of small electron dose and of extrapolation to zero bombardment time.

C. KBr

KBr was studied only in the monolayer and double layer range (Fig. 9). Both K and Br AES signals increase linearly up to 100 doses at which the K signal gives 3.65×10^{14} (K atoms)/cm^2, the Br signal 3.75×10^{14} (Br atoms)/cm^2, that is, stoichiometric KBr within the limits of error, with a total atomic density of 7.4×10^{14} atoms/cm^2. The AES slopes beyond 1 ML show the formation of a second layer. The decrease of $\Delta\phi$ at 185 doses suggests the beginning of the third layer or the nucleation of 3D crystals before completion of the double layer with twice the atomic density of the monolayer. The initial rapid linear change up to 20 doses $\hat{=}0.78\times10^{14}$ atoms/cm^2 for K and Br each can in principle again be attributed to upright or inclined KBr dipoles but the $\Delta\phi$ arguments are less compelling than in NaCl and KCl layers. The $\Delta\phi$ change expected from atoms in pure layers with the same coverage is -1.63 eV for the K and -0.32 eV for the Br atoms. This gives -1.95 eV for the KBr layer at 20 doses which is larger than the observed value of -1.73 eV. Thus an explanation in terms of a K+Br atomic gas is possible, even allowing for some depolarization. The ESD results to be discussed below, however, show a very pronounced K^+ ESD peak at low coverages which by analogy to NaCl and KCl is attributed to emission from KBr_n molecules (here $n=1$). In order to account for the observed $\Delta\phi=-1.73$ eV at a density of 0.78×10^{14} (KBr molecules)/cm^2, their $p_\perp^{KBr}$ must be 5.9 D ($p=26.1$ D for the free KBr molecule).

The condensation into 2D KBr islands is not well defined in the curve but can be deduced by analogy with NaCl (Fig. 2) from the ESD yield curves as a function of exposure (Fig. 10): the K^+ signal from the KBr gas disappears at about 30 doses and simultaneously a Br^+ and a weak K^+ signal appear, indicating island formation. The threshold for both K^+ and Br^+ ESD at higher coverages with energy distribution maxima at 3.2 and 2.4 eV, respectively, is 18 eV, that is, at the K 3p ionization energy (17.8 eV). No Br core level is involved up to the highest energy used (55 eV) but at the K 3s level a thresholdlike behavior is seen, at least in the K^+ yield (see Fig. 5).

In KCl layers the Cl^+ yield went to zero when the monolayer composition changed from KCl_2 to KCl with increasing bombardment time. Inasmuch as KBr grows stoichiometrically from the very beginning the much lower Cl^+ yield in the KBr monolayer may be a consequence of the stoichiometry. Therefore the composition was changed artificially by first depositing selected amounts of pure Br and subsequently adding sufficient K to complete the monolayer (total atomic density 7.5×10^{14} atoms/cm^2). Figure 11 shows the result of the K^+ and Br^+ yields, normalized to the respective K and Br coverages. Both have maxima for the composition K_7Br_5, Br^+ has a second maximum for the composition KBr_4 with comparable yield, and K^+ has a strong maximum at low K coverages, 15 times stronger than the K_7Br_5 K^+ maximum. Thus small deviations from 1:1 stoichiometry (K_7Br_5, K_9Cl_{10}) or a large excess of Cl are

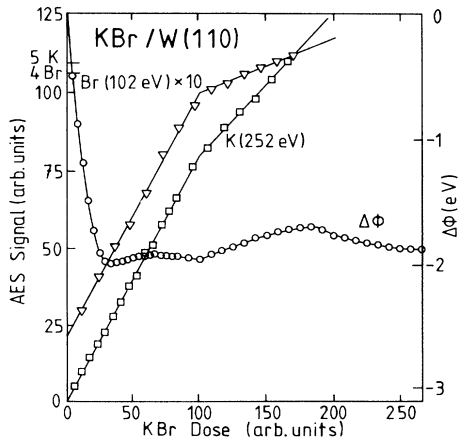

FIG. 9. Work-function change, Br 102-eV and K 252-eV Auger electron signals as a function of KBr exposure.

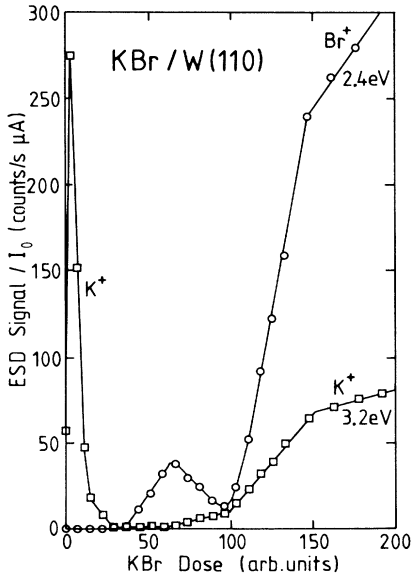

FIG. 10. ESD signals from KBr layers on W(110) as a function of KBr exposure.

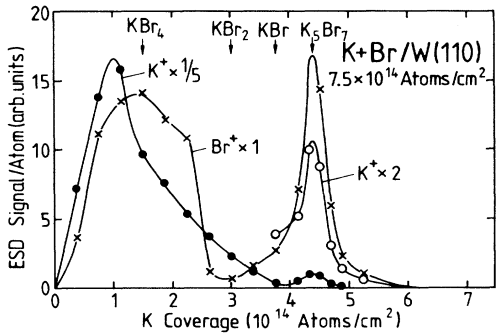

FIG. 11. ESD signals from mixed K+Br monolayers on W(110) as a function of K coverage.

favorable for ESD of ions but no ion ESD is observed for a large alkali excess ($n \geq 4$ in K_nBr), that is, low work function. For the composition KBr_2 the Br^+ yield/atom is small, $\frac{1}{25}$ of its value for the composition K_7Br_5. The composition MX_2 is obviously not the most ion ESD active. Compared to the Cl^+ yield/atom from the KCl_2 monolayer, the Br^+ yield/atom from a KBr_2 monolayer is by a factor of ≈ 6 smaller, compared to the Cl^+ yield/atom from the $NaCl_2$ layer at the maximum in Fig. 2 by a factor of ≈ 35.

D. KI

The AES signals of K and I in KI layers (Fig. 12) also increase linearly up to identical coverages, 3.45×10^{14} atoms/cm^2, giving a monolayer with composition KI and total atomic density 6.9×10^{14} atoms/cm^2. The small slopes of the AES signals above 100 doses are incompatible with ML-by-ML growth and indicate the formation of 3D crystals. While in KBr layers a ϕ minimum was hardly visible in the submonolayer range, a pronounced ϕ minimum is seen in KI layers at 30 doses corresponding to 1.05×10^{14} K and I atoms/cm^2 each. At these atomic densities pure K and I layers would cause a $\Delta\phi$ of -2.25 and -0.45 eV so that $\Delta\phi = -2.7$ eV would be expected for a 2D gas consisting of K and I atoms without mutual depolarization. The observed value $\Delta\phi = -2.4$ eV does not exclude this interpretation. The pronounced K^+ ESD signal below 30 doses (Fig. 13), however, suggests the same interpretation as for KBr layers, that is a KI molecular gas. From $\Delta\phi = -2.4$ eV and $n = 1.05 \times 10^{14}$ atoms/cm^2 the normal component $p_\perp^{KI} = 6.05$ D of the dipole moment of these molecules is obtained. (The dipole moment of the free KI molecule is 29.8 D.) After 2D condensation as indicated by the ϕ increase I^+ ESD sets in while strong K^+ ESD appears only in the second monolayer. The threshold for the 2.0-eV I^+ ESD from 100 to 200 doses is about 17.5 eV, which is within the limits of error equal to the K 3p ionization energy (17.8 eV). Weak 2.2-eV I^+ and 2.6-eV K^+ ESD is, however, already seen at 16.5 eV, so that a small contribution from I 5s ionization (13.6 eV) cannot be excluded. The 2.0-eV I^+ signal shows an additional thresholdlike increase at the K 3s ionization energy (33.9 eV) and the 2.6-eV K^+ signal increases much faster above this energy while no influence of K 3s holes on the 2.2-eV I^+ signal is seen.

The strong coverage dependence of the alkali-ion ESD yield Y_{M^+} in the 2D gas phase has been mentioned several times. In this region ϕ changes rapidly with coverage. It is, therefore, natural to attribute the strong variation of Y_{M^+} with ϕ not to changes in the M^+ creation process but to the destruction process via neutralization during escape from the surface, similar to the H^+ ESD yield dependence upon Cs coverage on W(110).[11] In order to check this hypothesis, the M^+ ESD yields at low coverages were studied in more detail and analyzed in terms of the resonance neutralization theory.[13] Figure 14 illustrates this for KI layers. The plot of the logarithm of the K^+ ESD yield/atom versus $\Delta\phi$ shows the shape typical for resonance neutralization

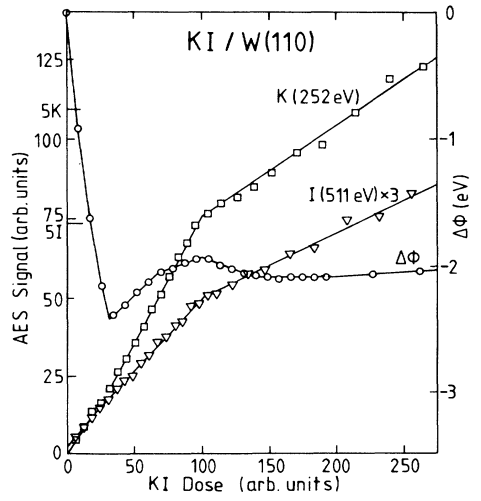

FIG. 12. Work-function change, I 511-eV and K 252-eV Auger electron signals as a function of KI exposure.

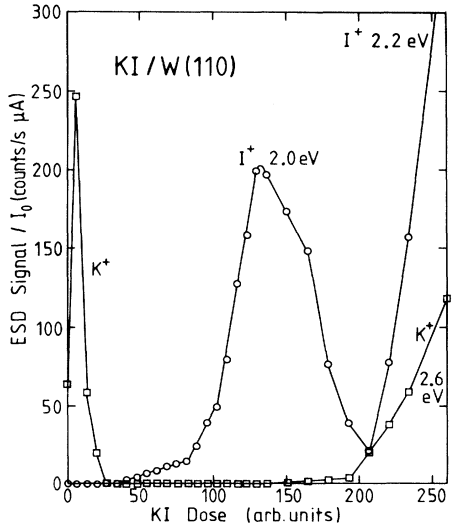

FIG. 13. ESD signals from KI layers on W(110) as a function of KI exposure.

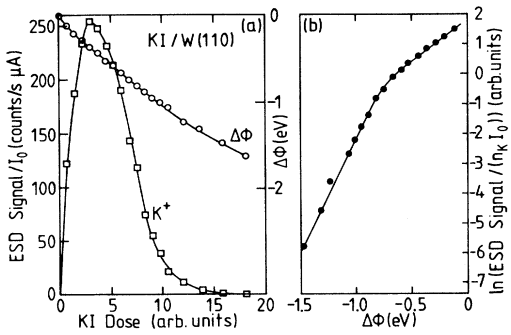

FIG. 14. (a) Low-coverage K^+ ESD signal from a KI layer on W(110) and work-function change as a function of KI exposure. (b) ln(K^+ signal/K atom) vs $\Delta\phi$ as obtained from (a).

which is also seen in H^+ ESD from W(110)+Cs (Ref. 11) and even better in the secondary ion yields from alkali layers on W(110).[8] In SI emission the ion creation process is not a bottleneck as it is in ESD so that the destruction process determines the ion yield.

E. CsI

CsI initially forms a monolayer, followed by 3D growth, similar to KI. This is seen in Fig. 15. The monolayer is, however, not stoichiometric CsI but contains 3.8×10^{14} (Cs atoms)/cm^2 and 3.0×10^{14} (I atoms)/cm^2, which gives within the limits of error the composition Cs_5I_4. $\Delta\phi(\theta)$ has a well-pronounced minimum at 44 doses ($\theta=0.44$). The saturation at 1 ML is a clear sign that the subsequent growth is three dimensional. The initial decrease can be approximated by two straight lines corresponding to two average dipole moments of the adsorbate with a transition between 0.1 and 0.2 ML. The linear region ends at 33 doses ($\frac{1}{3}$ ML) with a $\Delta\phi$ of -2.56 eV. If the adsorbate consisted of Cs and I atoms the $\Delta\phi$ data from the pure Cs and I layers would give $\Delta\phi=-(3.24+0.4)=-3.66$ eV if depolarization is neglected. Thus a 2D Cs+I atomic gas with strong depolarization is possible. No reliable information on possible Cs^+ ESD at low coverages is available because of an insufficient number of experimental points. The Cs^+ SI yield does not show the local maximum seen in the other halide layers[8] for which M^+ ESD has been observed at low coverages. Therefore we conclude that no upright or tilted CsI molecules exist below $\frac{1}{3}$ ML. Whether the 2D gas consists of Cs and I atoms or CsI molecules with the molecular axis parallel to the surface cannot be decided.

Similar to the other halides, X^+ ESD (Fig. 16) starts upon condensation at $\frac{1}{3}$ ML, reaches a maximum at 0.6 ML, and decreases to nearly zero at 1 ML. In the 3D growth region it increases very rapidly with coverage. No Cs^+ ESD could be detected in the monolayer range. In the initial phase of 3D growth the Cs^+ signal increases only slowly up to an average thickness of about 3 ML. Thereafter it rises very rapidly and even surpasses the I^+ signal. The threshold and energy distributions were measured only at large exposures (≥ 500 doses). In particular, the 3.5-eV Cs^+ signal appears first at about 50 eV, that is, at the I 4*d* ionization energy (49.6 eV) and increases much faster above the Cs 4*d* ionization energy (78.8 eV). At the largest exposure studied (875 doses) the 2.4-eV I^+ signal is only a small shoulder of the much stronger 3.5-eV Cs^+ signal (I^+:$Cs^+\approx1$:50). After short bombardment the 3.5-eV peak shifts to 4.0 eV and decreases at this energy rapidly with increasing electron dose.

IV. DISCUSSION

The results presented in Sec. III reveal a great complexity of the ESD process of ions from alkali halide layers on W(110). This complexity is not so much caused by

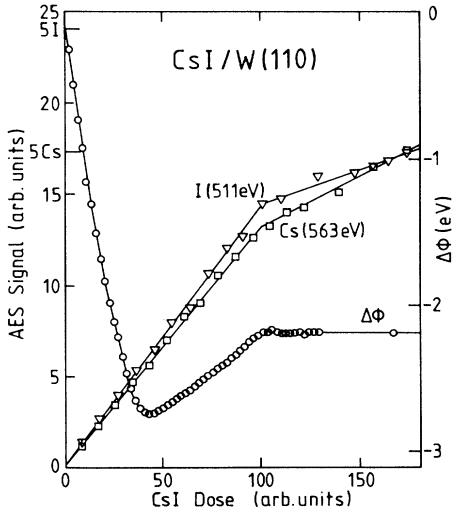

FIG. 15. Work-function change, I 511-eV and Cs 563-eV Auger electron signal as a function of CsI exposure.

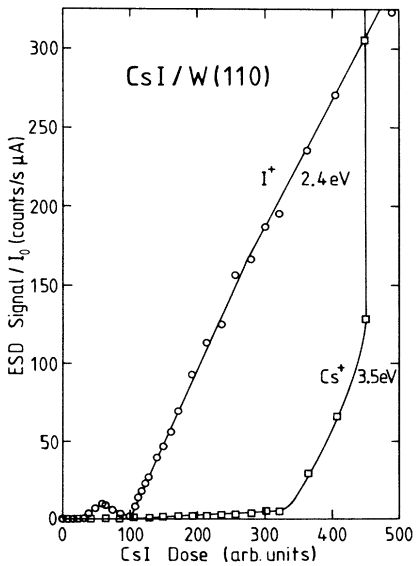

FIG. 16. ESD signals from CsI layers on W(110) as a function of CsI exposure.

the excitation process, which undoubtedly requires core level ionization. This is followed by intra-atomic or interatomic Auger deexcitation (Knotek-Feibelman mechanism) and creation of slow secondary electrons. It is rather a consequence of the influence of structure and composition on the possibility of excitation (interatomic transitions), on the localization of the excitation (atomic environment, long-range order, dimensionality, crystal size and shape, etc.), and on the survival probability of the ion (ϕ-, m-, and v-dependent neutralization probability).

We start with a discussion of the excitation process. Only for NaCl was an excitation curve for X^+ ESD from the transition layer ($NaCl_2$ monolayer) measured, all other curves were from thicker layers which are believed to be stoichiometric. In all cases, CsI excepted, the threshold for both M^+ and X^+ ESD was 17–18 eV. In NaCl Cl $3s$ ionization ($E_i = 17.5$ eV) creates the primary hole, in KBr and KI K $3p$ ionization ($E_i = 17.8$ eV), and in KCl both processes may be involved. In KI a weak contribution from I $5s$ ionization ($E_i = 13.6$ eV) cannot be excluded, but in CsI no evidence of this process is seen; rather, I $4d$ ionization (49.6 eV) determines the threshold. Several secondary thresholds are indicated such as Na $2p$ ionization ($E_i = 31.1$ eV) in the 1.0-eV Cl^+ ESD from the $NaCl_2$ monolayer, K $3s$ ionization ($E_i = 33.9$ eV) in K^+ ESD from thick KBr and in I^+ ESD from thick KI layers, and Cs $4d$ ionization ($E_i = 78.8$ eV) in Cs^+ ESD from CsI, but no systematic trend in the appearance of the secondary threshold is discernible. It appears that an energy of more than 23 eV must be available for ion ESD from CsI because holes with smaller ionization energies, e.g., Cs $5p$ ($E_i = 13.1$ eV), Cs $5s$ ($E_i = 22.7$ eV), and I $5s$ ($E_i = 13.6$ eV) have no significant effect. In the other, lighter halides 17 eV seem to be sufficient.

These observations immediately shed light on the ESD ion creation mechanism. If it were due to ionization of hyperthermal ESD neutrals, an increase in ESD ion yield should occur at all core levels thresholds because of the increase of secondary electron generation above them This is not observed. The dependence of Auger processes upon the combination of the electronic states involved can, however, easily explain the absence of ESD ion yield increases at specific core-level thresholds. A second argument against ionization of hyperthermal neutrals by secondary electrons will be given later.

Interatomic Auger transitions are the rule rather than the exception, e.g., for Na^+ from NaCl, Br^+ from KBr, I^+ from KI, or Cs^+ from CsI. The close neighborhood to the ion with the primary hole is always given in thick layers and in the condensed submonolayers and is, therefore, no bottleneck, but in the 2D gas phase the number of nearest neighbors is limited. Although no excitation functions for the 2D gas are available it appears reasonable to invoke interatomic Auger transitions also in this case whenever necessary for ESD.

The absence of X^+ ESD in this coverage region is easily explained by the model of upright or tilted MX_2 or MX molecules, with X providing the bonding to the substrate. An Auger process in the X^- atom can produce the necessary repulsive potential for M^+ ejection but not vice versa. Of the two models in the NaCl and KCl 2D gas phase, MX_2 and $MX+X$, we prefer the former for the following reasons: (i) the deposition temperature was always below the onset temperature of surface ionization,[10] (ii) even if surface ionization should occur it is difficult to understand why in all experiments with NaCl and KCl the composition 1:2 should always result, and (iii) the condensed 2D phase has the same composition. Many molecules lose part of their constituents upon chemisorption because of strong rearrangements caused by the bonding to the substrate. Thus the formation of an MX_2 transition layer during chemisorption of MX molecules is not surprising. Whether or not this is a specific feature of MCl adsorption can only be decided by studies of other M and X species. Here it was only observed for NaCl and KCl.

The conclusion from this study that the MX_2 and MX molecules are not parallel to the surface is also not unusual. There are numerous molecules, foremost CO, which are adsorbed upright or tilted. New are the large dipole moments which are possible in such layers, 6.75, 6.9, 5.9, and 6.05 D for $NaCl_2$, KCl_2, KBr, and KI, respectively. It is probably the large electrostatic energy of this dipole layer which causes the sudden flip-over of the molecules parallel to the surface and their rearrangement into a 2D condensate. The low dimensionality and the poor order in this condensate ensure poor delocalization of ion EDS-active excitations. Although no structural information is available, it can be assumed that each X atom in the MX_2 layer is surrounded by three M atoms which are surrounded by six X atoms on the average. Both M and X atoms lower ϕ so that the picture of an ionic layer with alternating positive and negative charges is not appropriate. The X atoms are covalently bonded to the substrate and may be considered to have zero charge. In an Auger process the X atom becomes doubly charged X^{++} ion which is in a strongly repulsive neighborhood. The lattice relaxation which suppresses X^+ emission in bulk alkali halides[3–5] is unlikely here because of the rigid W lattice and the strong bonding of the surrounding atoms to the substrate. Large X^+ ESD yields can, therefore, be expected in the monolayer range as seen in the $NaCl_2$ layer.

The strong composition dependence of the yields as seen in the increase from KCl_2 to K_9Cl_{10} and the rapid decrease towards KCl during Cl^+ ESD from the KCl_2 monolayer or in the sharp K^+ and Br^+ yield maxima at the composition K_7Br_5 in mixed K-Br monolayers (Fig. 11) cannot so easily be attributed to a favorable repulsive potential configuration of the emission site of the ion. More probably it is caused by better localization of the excitation due to chemical disorder. The strong continuous increase of the K^+ yield with decreasing K concentration in K-Br monolayers from very small values for KBr to a maximum and the subsequent rapid decrease (Fig. 11) has a different cause which can be understood best if one follows the K^+ yield curve in the opposite direction, i.e., in the direction of increasing K concentration and decreasing ϕ. Then the K^+ and $\Delta\phi$ curves look very similar to those shown in Fig. 14(a) and the K^+ yield dependence may be analyzed in the same manner: if

the logarithm of the K^+ yield divided by the K concentration is plotted as a function of $\Delta\phi$ a curve similar to that in Fig. 14(b) is obtained. This implies that the decrease of the K^+ yield with increasing K concentration above the maximum is caused by resonance neutralization of the ion after emission and not by some aspect of ion creation. Inasmuch as the K^+ yield plotted in Fig. 11 was already the yield per atom, dividing once more by the K concentration means that the K^+ yield/(K atom) is proportional to the number of K atoms. Thus the K^+ yield increases with increasing number of K neighbors, i.e., with increasingly repulsive environment as one would expect. The observed decrease with increasing K concentration is solely caused by postemission neutralization which increases strongly with decreasing work function.

There are many other details in the low-coverage range worthy of discussion but we will now conclude this section with the main problem which motivated this study, ESD of ions from bulk ionic crystals. Of course even the thickest layers studied, 20 ML for NaCl and 2–5 ML for the other alkali halides, are still far from the bulk. In all cases we went past the initial transition layer but the material in excess of it was poorly ordered and the 3D crystals were certainly very small. Nevertheless, a substrate influence should have been absent in the thickest layers and they should have been stoichiometric. In all these layers strong ESD of energetic ions was observed, with the general tendency of increasing ion energy and decreasing ion yield with increasing mass. This is what one would expect if the yield is strongly influenced by postemission neutralization because with increasing mass the velocity decreases for a given energy—and thus the neutralization probability increases—and for larger mass the energy must be larger so that the necessary escape velocity is available. There are some deviations from this general trend whose understanding requires detailed additional studies.

The observed ESD of ions from thick layers is in apparent disagreement with the theoretical predictions that ionic desorption from rocksalt-type crystals is very unlikely because of lattice relaxation.[3–5] Postemission ionization of neutrals by secondary electrons which has been invoked to explain the measurable ion yield from bulk crystals[6] can be excluded to make a significant contribution in our case because some of the strongest ESD signals such as the Na^+ signal from NaCl (Fig. 3), the Br^+ signal in KBr (Fig. 10), and the I^+ signal in KI (Fig. 13) appear only upon ionization of a core level in the corresponding neighbor atom (Cl and K, respectively). The concentration of molecules in the gas phase is too small to be able to account for this process after neutral molecule emission. The disagreement with theory could be only an apparent one. First of all, our films have many atoms in ledge and other poorly coordinated positions in contrast to the atoms in the (100) surface treated in the theory. Secondly, several mechanisms, though rare, allow ion emission also within the framework of the molecular dynamics calculations, and thirdly these calculations do not fully take into account all aspects of the ESD process but concentrate on the dynamics of the ion or atom. Another approach which emphasizes the electronic aspects of the process predicts emission of energetic ions from small clusters simulating (100) surfaces.[14]

Our results leave no doubt that direct ion ESD from alkali halides is possible without postionization of neutrals. Neutral emission via excitation processes in the bulk and various transport processes to the surface, such as "hot valence hole" diffusion[15] could not be observed in thin films anyway.[16] In view of our results it appears certain that the Na^+ ESD from bulk NaCl crystals above the Cl 3*s* threshold, which was observed at 200 °C after preirradiation with faster electrons[7] is of the same nature as observed here in thick films and was *not* produced by postionization of emitted neutrals as suggested in more recent work.[6]

The question remains: why is ESD of ions from bulk alkali halides so elusive? There are some obvious experimental reasons such as alkali accumulation on the surface if the temperature is too low for thermal alkali desorption. This alkali layer suppresses ion emission by efficient neutralization due to its low work function. A second experimental problem is surface charging of the insulating bulk alkali halide crystals. However, there is also a possible fundamental cause for the dominance of neutrals in the nonthermal component of the emission: neutralization. The results for Cl^+ ESD from the NaCl monolayer and of K^+ ESD from KBr monolayers clearly indicate the importance of postemission neutralization. Alkali halides have a large secondary electron (SE) yield. The SE distribution of alkali halides peaks at about 1 eV (Ref. 17) so that a significant fraction of the SE's is unable to ionize neutrals but able to neutralize ions. Ionization of halogen atoms is negligible up to electron energies of 10 eV and more[18] while neutralization by electron capture is quite efficient in the 1-eV range. The published data for KCl actually tell us that the vast majority of SE's have energies below 10 eV: 90% of them have energies below 6 eV,[19] the half-width of the energy distribution is 4 eV (3.5 eV) with the maximum at 1 eV (1.4 eV).[17,20] SE energy distributions with negligible emission above 6 eV have also been reported for soft x-ray-induced SE emission form all the alkali halides discussed here.[21] Recent measurements[22] confirm these results also for SE induced by electrons in the 100-eV range. For example, in KCl less than 2% of the SE's have energies above the ionization threshold of Cl. Thus neutralization is expected to dominate ionization. Accordingly the experiments in which ESD ion emission of Na^+, Cl^+, and of molecular ions from a bulk NaCl crystal was attributed to ionization of emitted neutrals by SE's[6] could also be construed as evidence for efficient neutralization of ESD ions by slow SE's producing an abundance of neutrals. Even negative ESD ion formation can be explained in this manner by electron attachment. Similarly, the recently reported nonthermal halogen atom ESD along the ⟨100⟩ direction of KCl and KBr crystals which lead to the "hot valence hole" model of neutral atom ESD (Ref. 15) can be attributed to neutralization of ESD ions by slow SE's. The lower energies of these atoms compared to those found here in the thick KCl and KBr layers is not surprising in view of the different measurement techniques involving possibly zero-energy differences. Also the non-normal

emission from {110} surfaces is not in contradiction to the neutralization hypothesis because these surfaces facet into {100} surfaces upon hating to 700 K.[23] Ion emission normal to these surfaces followed by neutralization leads to the observed emission at 45° with respect to the {110} surface normal.

V. SUMMARY

The study of the electron-stimulated desorption of ions from thin alkali halide layers on W(110) and the supporting AES and $\Delta\phi$ studies for the characterization of these layers have uncovered a wide range of physical phenomena involving not only electronic excitations in ionic solids and their conversion into ionic energy but also the growth of thin ionic layers on metal surfaces. A molecular gas phase has been found to precede the formation of a 2D condensed layer which is followed by a second (KCl, KBr) or more layers (NaCl) or 3D crystals (KI, CsI). The first two layers of NaCl and KCl contain an excess of Cl, the first CsI layer an excess of Cs. Electron-stimulated desorption of ions from these layers occurs via the Knotek-Feibelman mechanism and is strongly structure and composition dependent. A detailed analysis of the dependence of the ion yields on structure and composition of the layers allows a partial disentanglement of the various factors which determine ion emission after electronic excitation, that is, excitation localization, repulsive potential formation, and neutralization. Neutralization is seen to play an important role and should be taken into account in modeling the emission of fast neutrals from bulk alkali halides.

[1]Ph. Avouris and R. E. Walkup, Annu. Rev. Phys. Chem. **40**, 173 (1989).
[2]R. D. Ramsier and J. T. Yates, Jr., Surf. Sci. Rep. **12**, 243 (1991).
[3]R. E. Walkup and Ph. Avouris, Phys. Rev Lett. **56**, 524 (1986).
[4]A. E. Kiv, A. A. Malkin, and M. A. Elango, Fiz. Tverd. Tela (Leningrad) **28**, 1856 (1986) [Sov. Phys. Solid State **28**, 1032 (1986)].
[5]T. A. Green, M. E. Riley, and M. E. Coltrin, Phys. Rev. B **39**, 5397 (1989).
[6]R. E. Walkup, Ph. Avouris, and A. P. Ghosh, Phys. Rev. B **36**, 4577 (1987); in *Desorption Induced by Electronic Transitions, DIET III,* edited by R. H. Stulen and M. L. Knotek (Springer, Berlin, 1988), p. 248.
[7]T. R. Pian, M. M. Traum, J. S. Kraus, N. H. Tolk, N. G. Stoffel, and G. Margaritondo, Surf. Sci. **128**, 13 (1983).
[8]U. Stawinski, Ph.D. thesis, Technische Universität Clausthal, 1989.
[9]M. Szymonski, in *Desorption Induced by Electronic Transitions, DIET IV,* edited by G. Betz and P. Varga (Springer, Berlin, 1990), p. 270.
[10]F. Bonczek, T. Engel, and E. Bauer, Surf. Sci. **94**, 57 (1980).
[11]M.-L. Ernst-Vidalis, C. Papageorgopoulos, U. Stawinski, and E. Bauer, Phys. Rev. B **45**, 1793 (1992).
[12]K. P. Huber and G. Herzberg, *Molecular Spectra and Molecular Structure* (Van Nostrand Reinhold, New York, 1979), Vol. IV.
[13]N. D. Lang, Phys. Rev. B **27**, 2019 (1983).
[14]N. Itoh, A. M. Stoneham, and A. H. Harker, Surf. Sci. **217**, 573 (1989).
[15]M. Szimonski, J. Kolodziej, P. Czuba, P. Piatkowski, A. Poradzisz, N. H. Tolk, and J. Fine, Phys. Rev. Lett. **67**, 1906 (1991).
[16]M. Szymonski, T. Tyliszczak, P. Aebi, and A. P. Hitchcock, Surf. Sci. **271**, 287 (1992).
[17]K. H. Geyer, Ann. Phys. (Leipzig) **41**, 117 (1942).
[18]T. R. Hayes, R. C. Wetzel, and R. S. Freund, Phys. Rev. A **35**, 578 (1987).
[19]E. J. Sternglass, Rev. Sci. Instrum. **26**, 1202 (1955).
[20]Lan Yu Huang, Z. Phys. **149**, 225 (1957).
[21]B. L. Henke, J. Liesegang, and S. D. Smith, Phys. Rev. B **19**, 3004 (1979).
[22]F. Golek and E. Bauer (unpublished).
[23]E. Bauer (unpublished).